

Effects of the Butterfly Forewing Flap-and-twist Motion on the Generation of Thrust and Lift

Kamonrat Tangudomkit and Pruittikorn Smithmaitrie *

Department of Mechanical and Mechatronics Engineering, Faculty of Engineering, Prince of Songkla University, Hat Yai, Songkhla, Thailand; Email: 5810130007@psu.ac.th (K.T.)

*Correspondence: pruittikorn.s@psu.ac.th (P. S.)

Abstract—A butterfly is a unique flying insect that can fly at a low flapping frequency of 10-15 Hz. Therefore, it consumes little energy while flying. However, the mechanism of low-frequency wing beat has not been thoroughly explained. In this work, it was found that the synchronized flap-and-twist motion enhances the positive lift during both upstroke and downstroke. Models of butterfly forewings were made and tested to investigate the effects of flapping and twisting motions on the generation of thrust and lift. The active flapping and passive twisting mechanisms are proposed. Different ranges of flapping and twisting angles of the wings were investigated. The experimental result shows that the large symmetric twist angle $[-75^\circ, 75^\circ]$ has a unique 3-cycle repetition of flapping force, which generates positive lift in a range of 0-0.06 N most of the time, with strong thrust fluctuations in a range of ± 0.10 N. This synchronized flapping and twisting motion with positive lift generation is one explanation for butterfly flight in nature and reveals how butterflies can lift themselves with such a low flapping frequency.

Keywords—flapping wing, butterfly robot, aerodynamics, wing synchronous motion

I. INTRODUCTION

The mechanism of wing flapping has long been an interesting research topic. Inspired by nature, people have tried to study and imitate flying animals such as birds [1], [2], dragonflies [3], butterflies [4]–[7], beetles [8], and bees [9]. All of the invented flying robots can generate thrust and lift forces greater than their own weight and fly themselves in the air. However, the aerodynamics of the robot's flapping mechanisms are different from those of animals. The wing structure and motor drive are also different from bones and muscles. Therefore, studies on the generation of thrust and lift forces need to be conducted on various invented artificial wings to better understand flight and improve the flight efficiency of robots that mimic nature.

A butterfly is a flying insect that can fly with a low flapping frequency of 10–15 Hz. The wing beat is much lower than the wing beat of other insects, usually 200–300 Hz. The low frequency wing beat consumes little energy [10]. There are some variations in insect wingbeat mechanisms. Insects have two pairs of wings, one pair on

each side of the body. Most insects flap their forewings and hindwings synchronously. However, there are some insects, such as dragonflies and butterflies, that can control their forewings and hindwings separately. The dragonfly has complete control over its four wings, which it can beat, independently. This allows dragonflies to fly in any direction. Butterflies can also control the flapping of the forewings and hindwings by bending their bodies to control the angle of attack of the forewings and the overlap of the wings. Butterfly wings can flap up and down, and also twist to change the angle of attack as needed [11,12]. An experimental study of a 3D flapping wing has shown that the wing twisting affects the aerodynamic force [13]. On the other hand, butterfly robots have been continuously developed by many researchers. Butterfly robots generally fly with a Reynolds number of 10^5 – 10^6 [5], [14], [15]. T. Fujikawa *et al.* studied the flapping motion [4] and flight characteristics of a butterfly robot [16], [17] by numerical simulations and conducting trajectory monitoring experiments. The results showed that a butterfly moves its abdomen upward when flying upward and moves its abdomen downward when flying forward. The flight characteristics were controlled by different inclination angles of the body. It was found that the unsteady vortices generated the lift. H. Tanaka *et al.* studied various aerodynamic parameters of a mimic swallowtail butterfly, including aerodynamic force, angle of attack (AOA) [18], wing venation [19], and aerodynamic flow [18]. The AOA and wing venation were found to affect wing deformation and aerodynamic flow. Kovac *et al.* studied the effects of butterfly wing shape on the generation of lift and drag [14]. The result showed that the natural wing shape has better glide performance than the non-natural wing shape because the natural wing shape generates the larger lift force. Chen *et al.* demonstrated the lift force and aerodynamic flow of a butterfly robot by mimicking a dead leaf butterfly [5]. The airflow investigation was performed using the PIV technique. The results have shown that the robot generates only one-eighth of its body weight in lift force, which is insufficient for flying. According to the aforementioned works, research on butterfly robots is quite limited in terms of topics and specific areas of interest

compared to research on bird robots. The study of parameters that generate lift and thrust, such as passive wing twisting during wing flapping, has never been conducted. This topic is a key factor that makes the butterfly flapping unique and would reveal the understanding of the natural wing twisting function of the butterfly wing beat.

This work focuses on the effect of wing twist angle on the generation of thrust and lift using a model of a swallowtail butterfly wing, and proposes a new synchronized flap-and-twist mechanism. The detailed study is presented next.

II. THE BUTTERFLY THRUST AND LIFT GENERATION

Unlike bird robots, the generation of thrust and lift in the butterfly robot depends on two effects caused by wing motion. These are the effects of added mass and wing twisting. The effect of added mass or virtual mass occurs during upstroke when the wing moves with acceleration and suddenly decelerates. The inertia of the wing mass and the surrounding air contribute to lift the wing and the body to continue the motion in the previous direction [20]. However, the added mass effect occurs in insects that are capable of changing the angle of attack of the wings, such as hoverflies, dragonflies, hawkmoths, and fruit flies [21]. The force due to added mass is difficult to measure separately because it is combined with the thrust effect.

In addition to the added mass effect, the effect of wing twisting passively changes the angle of attack and the air outlet area. When the wing rapidly flaps, it draws the front air and releases it at the rare. The released air with increased velocity due to the wing perturbation causes the propulsion with the reaction force in the opposite direction to the jet stream. This is the thrust generation. The thrust (T) depends on the velocity of the outflowing jet and the cross-sectional area of the jet. It can be written as

$$T = \frac{1}{2} C_T \rho V_{jet}^2 A_o \quad (1)$$

where C_T is the thrust coefficient, ρ is the air mass density, V_{jet} is the velocity of the air outflow, and A_o is the air outlet area.

III. THE FLAP-AND-TWIST MECHANISM AND WING MODEL

To mimic the butterfly flapping motion and to investigate the generation of thrust and lift, a new butterfly flapping mechanism is introduced in this study. The proposed flap-and-twist mechanism of a butterfly forewing model was designed and fabricated. The size of the forewing model is twice the size of the forewing of the *Papilio Helenus Mooreanus* butterfly [22] as shown in Fig. 1.

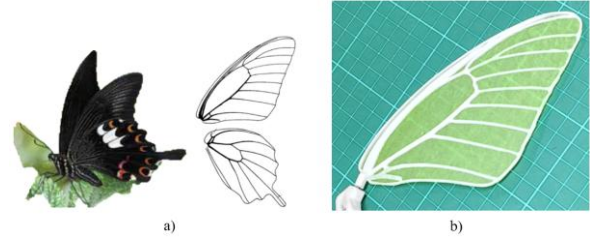


Figure 1. a) The *Papilio Helenus Mooreanus* wing shape [22] and b) the butterfly forewing model.

The flap-and-twist mechanism has 2 degrees of freedom: one rotation about the flapping axis and another rotation about the twisting axis. The design of the flapping and twisting mechanism of the butterfly forewing model is shown in Fig. 2. The system consists of a DC motor, a flap-and-twist mechanism, and a forewing model. The DC motor rotates a crank connected to a two-bar linkage mechanism to control a wing flapping mechanism. The specification of the motor is described later in the experimental setup.

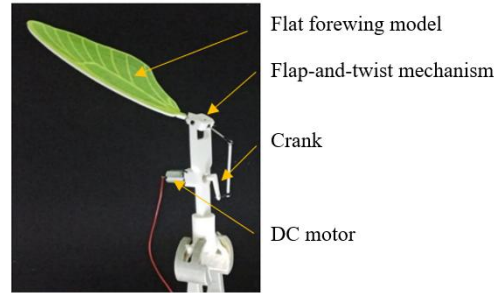
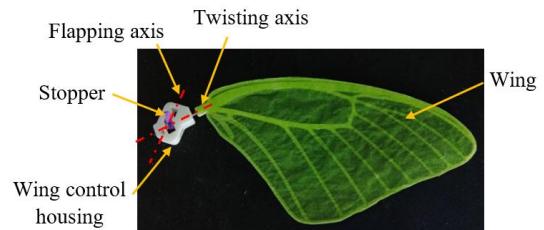


Figure 2. The flapping and twisting mechanism of the butterfly forewing model.

The passive twisting range of the wing is controlled by the slot and stopper inside the wing control housing, as shown in Fig. 3. The passive twisting motion of the wing about the twisting axis is caused by the unbalanced drag acting on the wing surface. The slot-and-stopper mechanism limits the range of the twist angle that controls the air outlet area. Consequently, thrust can be controlled by changing the air outlet area according to Eq. (1). To study the synchronization effect of wing flapping and twisting, the flap-and-twist mechanism was designed to create active-flapping and passive-twisting actions in different ranges of twisting motion. In nature, wing twisting in butterflies occurs only on the forewing, not on the hindwing. Therefore, the forewing model is considered in this paper.



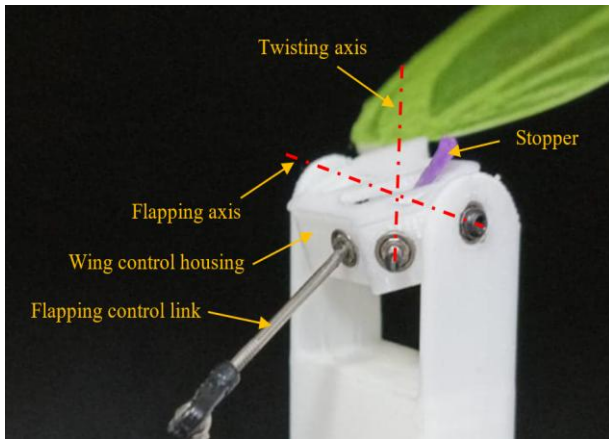


Figure 3. The active-flapping and passive-twisting mechanism.

The wing width and thickness of the wing venation are shown in Fig. 4. The forewing model was fabricated by using the fused modeling (FMD) method with a 3D printer (PRUSA i3 MK3) and PLA plastic material (PLA+). The wing membrane with a thickness of 0.02 mm is made of straw paper, which was attached to the wing venation with adhesive. The design and fabrication method of the forewing model are summarized in Fig. 5. The specifications of the butterfly wing and the forewing model are listed in Table I. The experimental setup is explained in the next section.

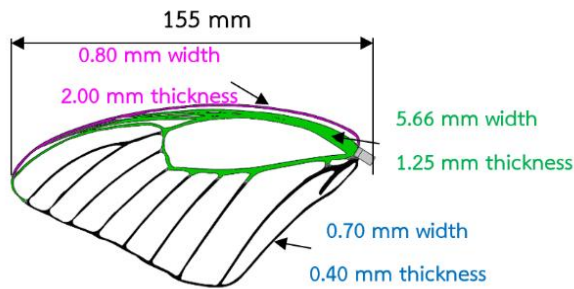


Figure 4. Dimension of the forewing model.

TABLE I. SPECIFICATIONS OF THE BUTTERFLY WING AND THE FOREWING MODEL

Specifications	Papilio Helenus Mooreanus	Forewing model
Weight	~ 0.3 g (a large butterfly)	2.36 g
Forewing length	55–65 mm	155 mm
Venation thickness	N/A	0.4–2.0 mm
Venation weight	N/A	2.18 g
Wing membrane thickness	N/A	0.02 mm
Wing membrane weight	N/A	0.18 g

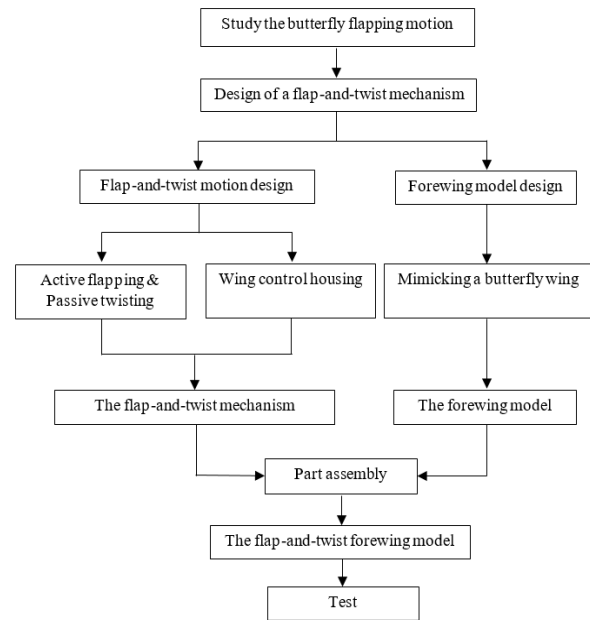


Figure 5. Design and fabrication method of the forewing model.

IV. EXPERIMENTAL SETUP

The experiments to study the butterfly forewing model were set up as follows to investigate the wing motion and aerodynamic parameters.

The flap-and-twist mechanism creates the wing flapping pattern by combining upstroke and downstroke with wing twisting. In the experiment, the flapping angle (θ) ranged from -40° to $+20^\circ$, as shown in Fig. 6(a). The forewing was free to rotate and change the angle of attack with the twist angle (α), as shown in Fig. 6(b). The range of twisting motion depended on the length of the slot in the flap-and-twist mechanism. In this study, six models of the wing control mechanism allowing different ranges of wing twist angle (Table II) were used to investigate the effects of the flap-and-twist motion on the generation of thrust and lift.

TABLE II. THE MODELS OF THE FLAP-AND-TWIST MECHANISM

Model	Twist angle range
1. Non-twist angle	$[0^\circ, 0^\circ]$
2. Twist angle	$[-45^\circ, 30^\circ]$
3. Large twist angle	$[-55^\circ, 45^\circ]$
4. Unsymmetrical twist angle	$[-90^\circ, 10^\circ]$
5. Unsymmetrical twist angle	$[0^\circ, 100^\circ]$
6. Symmetrical twist angle	$[-75^\circ, 75^\circ]$

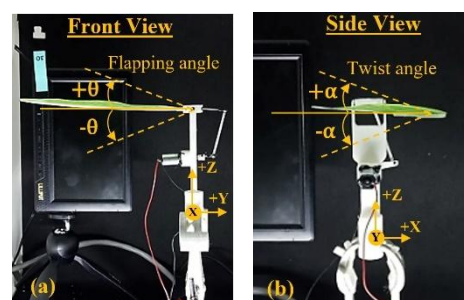


Figure 6. Front and side views of the forewing model.

The experimental setup shown in Fig. 7 consists of the butterfly forewing model with flap-and-twist mechanism, a DC motor, a three-axis force and torque sensor (ATI Industrial Automation, model: Gamma), a laptop computer with an extended monitor display, a power supply (KBM Engineering, PS-3003), and a high speed video camera (Sony Cyber-Shot DSC-RX 100V). The reaction force due to the flapping and twisting behavior was measured by using the triaxial force sensor installed on the fixed base. The wing motion was recorded with a high-speed video camera. By recording the data synchronously, the relationship between the generated force and the wing motion can be determined.

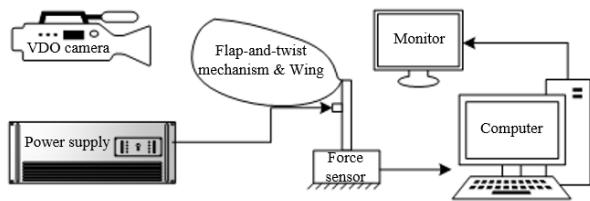


Figure 7. The experimental setup.

The 6V power supply was connected to the DC motor that drives the crank and the flap-and-twist mechanism. The 6V DC motor with the gearbox has a no-load speed of 200 rpm and maximum torque of 80 g-cm. The forewing model, flap-and-twist mechanism and motor were supported and mounted on the force sensor as shown in Fig.8. The measured force and VDO recording data show the forewing beat in action, the synchronization of the wing flapping and twisting, and the generated thrust and lift forces. The sampling frequency of the force and torque sensor was 1,000 Hz. The wing motion was recorded by the high-speed camera at 1,000 fps. The initial position of the wing was in the bottom position for all tests. The measurement data and the movement of the wing were recorded synchronously for 3 seconds and each measurement was repeated five times. The measurement data and the initial time of the measurement are synchronized at the wing bottom position. Thus, the measurement data from the repeated experiments can be averaged.

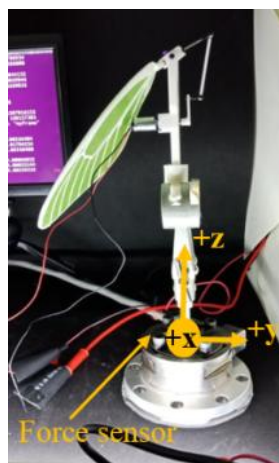


Figure 8. The flap-and-twist wing model and the force sensor.

This study focuses on the effects of the butterfly forewing flap-and-twist motion on the generation of thrust and lift. The tested forewing model on a fixed base does not exhibit the flight characteristics of a complete robot. Hence, other aerodynamic parameters, such as Reynolds number (Re), reduced frequency (k) and wing loading that are directly related to a flying robot could be further investigated in a final robot design.

V. RESULTS AND DISCUSSION

The generated force and wing motion were recorded while the wing was flapping. The experimental results of each model are presented as follows,

A. Model 1: Flapping with Non-twist Angle $[0^\circ, 0^\circ]$

Model 1 with an α -range of $[0^\circ, 0^\circ]$ represents the flat flapping wing without twisting, i.e., the slot-and-stoper mechanism is fixed at $\alpha=0^\circ$. The flapping action and generated forces were recorded as shown in Figs. 9 and 10, respectively. The red line in Fig. 9 represents the extended flapping axis, which indicates the wing flapping angle. The result shows that the wing position moves in a range between $+25^\circ$ stroke up and -50° stroke down. This range is larger than the expected crank mechanism design of $[+20^\circ, -40^\circ]$ due to the wing inertia, structural bending, and air resistance effects.

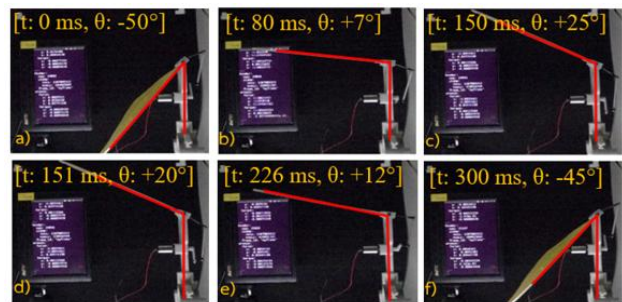


Figure 9. The flapping motion without wing twisting.

Fig. 10 shows the average flapping force components in the x-, y- and z- directions. The wing began to move upward from the bottom position at -50° and reached the top position at $+25^\circ$ in 151 ms and began to move downward to complete a flapping cycle. The flapping period was 300 ms. That is, the flapping frequency was 3.3 Hz.

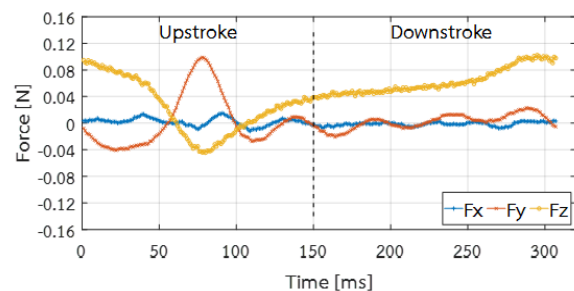


Figure 10. The flapping force components of the Model 1, non-twist angle $[0^\circ, 0^\circ]$.

The result of the force components in Fig. 10 shows that the maximum lateral force of 0.1 N in the y-direction was generated in the middle of the upstroke movement. The lateral force was generated by a single side wing. The lateral force could be canceled by the opposite wing, as found in a previous study [23]. The minimum lift force in the z-direction of -0.04 N occurred when the wings were fully extended in the middle of the upstroke. The lift force was positive most of the time except when the wing was spread during 60-100 ms or 20%-33% of the flapping cycle. This means that without twisting, the wing generates positive lift most of the time. On the other hand, the forward thrust in the x-direction fluctuated around zero all the time. Therefore, the effective lift is higher than the effective thrust of the non-twist forewing design. The high lift generation is suitable for the jump takeoff, which consumes less energy than the initial velocity takeoff. This behavior reflects the butterfly flight, which can rise vertically and fly at a low flapping frequency because the butterfly's forewings can generate the high lift.

B. Model 2: Flapping with the Passive Twist Angle [-45°, 30°]

Model 2 was developed to study the effects of passive twist angle (α) in the range of -45° to 30°. In this case, the wing can rotate about the flapping axis and twisting axis. The wing motion is shown in Fig. 11. The wing started in the bottom position. During the upstroke motion, the drag resisted the wing motion, so the wing twisted with positive angle of attack and the wing top position was reduced to $\theta = 10^\circ$, instead of 20° (Fig. 11(b)) with respect to the position of the flapping control link. Later, during the downstroke motion, the twist angle eventually became a negative angle of attack due to the air resistance pushing the wing in the opposite direction. The trailing edge of the wing aligned with the leading edge as the wing began to change direction from upstroke to downstroke or vice versa, as shown in Figs. 11(c) and (f).

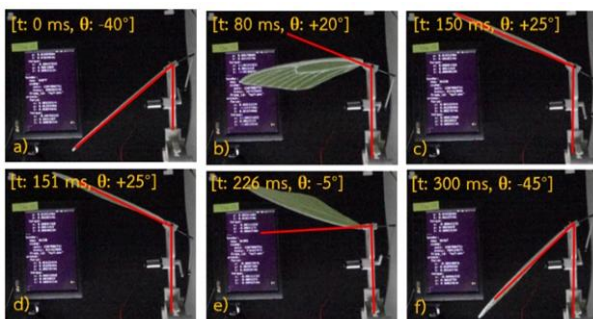


Figure 11. The flapping motion with the passive twist angle range [-45°, 30°].

The generated force components in all directions are shown in Fig. 12. The maximum force of 0.12 N occurs in the lateral direction, as in the previous case. However, the magnitude of the lift force was significantly reduced. This means that the passive wing twist motion is not able to hold the structural rigidity of the wing against the air resistance to generate the lift force. However, the magnitude of the forward thrust fluctuation increased compared to the

previous test. This event reveals that the passive twist motion converts vertical lift into horizontal thrust by rotating the forewing and deviating the airflow. This can be seen in the air outlet, which was opened wider by the wing twisting.

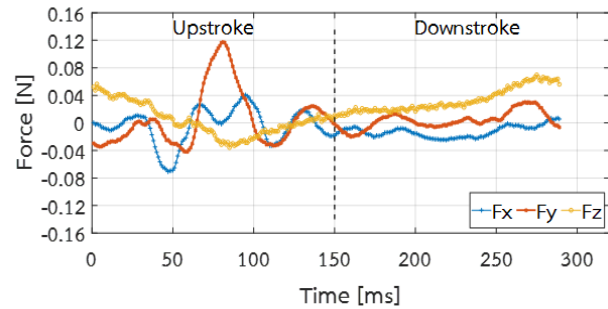


Figure 12. The flapping force components of the Model 2 with the passive twist angle [-45°, 30°].

C. Model 3: Flapping with Large Passive Twist Angle [-55°, 45°]

The twist angle of Model 3 was modified by increasing the range of the wing twist angle to [-55°, 45°], while the flapping angle remained the same. The objective was to investigate the generation of thrust and lift when the passive twist angle is increased. The result of the wing motion is shown in Fig. 13. In Figs. 13(b) and (e), it can be clearly seen that the wing was twisted more than the previous model due to air resistance. The result of the generated force in Fig. 14 shows a similar trend to the previous case. However, the lateral force fluctuation increases, the lift decreases slightly, and the thrust fluctuation increases. The fluctuation of thrust is more obvious when the passive twist angle increases.

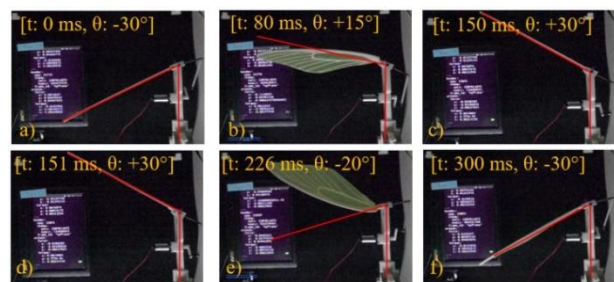


Figure 13. The flapping motion with the passive twist angle range [-55°, 45°].

The force components in Fig. 14 show that the fluctuation of the force magnitude in the x- and y-directions has increased dramatically compared to the previous model. However, the oscillation frequency and trend were still the same. The maximum lateral force of 0.14 N occurred at the midpoint of the upstroke. The thrust oscillation ranged from -0.12 to 0.10 N. This confirms that the passive twist angle affects the conversion of lift-to-thrust. However, a large passive twisting angle reduces lift and causes a large lateral force that is not conducive to forward flight.

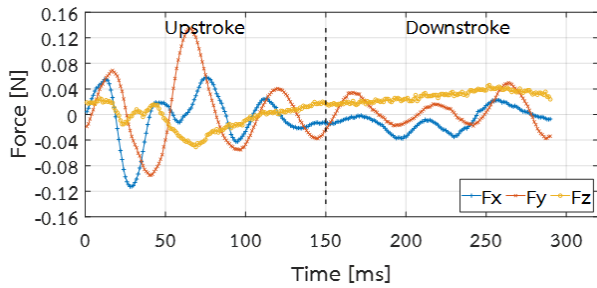


Figure 14. The flapping force components of the Model 3 with the passive twist angle $[-55^\circ, 45^\circ]$.

D. Model 4: The Unsymmetrical Twist Angle $[-90^\circ, 10^\circ]$

Model 4 was developed to study the flapping of the forewing when the unsymmetrical passive twist angle occurred. In this case, the range of twist angle is $[-90^\circ, 10^\circ]$. That is, the wing can open an angle of attack of up to 90° at upstroke and has a closed angle of attack of 10° at downstroke. The flapping motion is shown in Fig. 15. It can be easily noticed that the synchronization between the flapping and twisting motions has changed compared to Models 2 and 3. The first alignment of the trailing part of the wing and the leading edge occurred late in the middle of the downstroke, instead of at the beginning of the downstroke as in the previous case. In addition, the second alignment cannot be seen. The lack of correspondence between the flapping and twisting motions affected the generated force, as shown in Fig. 16. The peak lateral force decreased to 0.07 N and the timing shifted to the transition between upstroke and downstroke. The lift decreased slightly, and the thrust was barely generated. The thrust and lift varied within a narrow range of ± 0.04 N. This means that this model is not suitable for real flight.

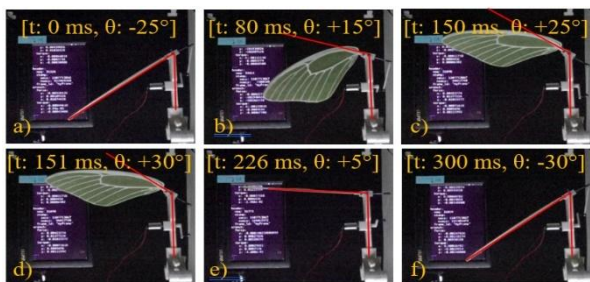


Figure 15. The flapping motion with the passive twist angle range $[-90^\circ, 10^\circ]$.

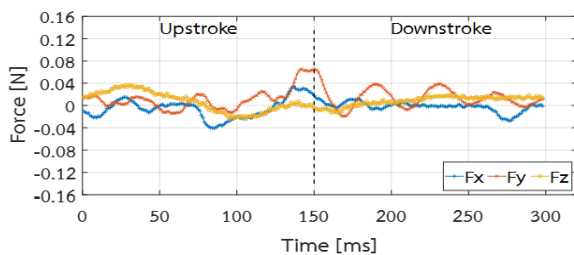


Figure 16. The flapping force components of the Model 4 with the passive twist angle $[-90^\circ, 10^\circ]$.

E. Model 5: The Unsymmetrical Twist Angle $[0^\circ, 100^\circ]$

Model 5 is the forewing model with unsymmetrical passive twist angle on the opposite side of Model 4 because the goal is to study the effects of closed angle of attack during downstroke. The wing can close the angle of attack only during downstroke, and the maximum closed angle is 100° . The wing cannot open the angle of attack during upstroke. With a large twist angle during downstroke, the trailing air outlet area increases. However, the leading air intake area remains about the same as in Model 1 without a twist angle. The flapping motion of the wing in Fig. 17 shows that the trailing part of the wing aligns with the leading edge during upstroke due to the structural constraint. During downstroke, the trailing part of the wing cannot move as fast as the leading edge due to the inertia of the wing and the slot-and-stopper mechanism, which allows a large passive twist angle as shown in Figs. 17(c) to (f).

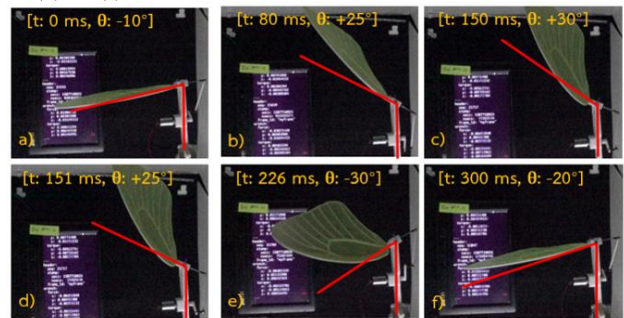


Figure 17. The flapping motion with the passive twist angle range $[0^\circ, 100^\circ]$.

The force components were measured as shown in Fig. 18. Model 5 generated the most oscillatory force during upstroke. The major contribution was the thrust component (F_x). The negative lift was caused by drag pushing against the non-twisted wing during upstroke. The upward moving wing structure deflected the air to flow rearward, resulting in a thrust fluctuation in the range of ± 0.08 N. During downstroke, the wing with the large passive twist angle could not generate any significant force because the twisted wing could not resist the airflow. Therefore, it could not generate any useful reaction force.

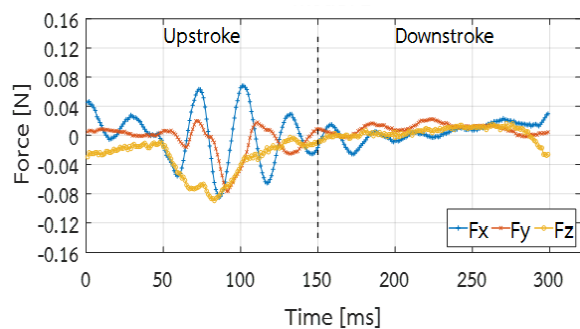


Figure 18. The flapping force components of the Model 5 with the passive twist angle $[0^\circ, 100^\circ]$.

F. Model 6: The Unsymmetrical Twist Angle $[-75^\circ, 75^\circ]$

Model 6 was designed to investigate the effects of a large symmetrical twist angle on the generation of thrust and lift. The twist angle range is $[-75^\circ, 75^\circ]$. During the flapping test, it was found that the generated force was repeated every three flapping cycles. This trend of force response had not occurred in the previous models. The results of the flapping motion in three cycles are shown in Fig. 19. The synchronized flap-and-twist motion was stable after a few flapping cycles. The beginning of a flapping cycle was counted when the flapping axis was in the bottom position (Fig. 19(a)). The wing was in the closed angle of attack configuration due to drag. Later, at the beginning of the upstroke (Fig. 19(b)) the wing and leading edge were aligned. Examination throughout the flapping motion showed that the wing blade followed the leading edge most of the time, except when the wing was in downstroke, Fig. 19(j) - Fig. 19(l) of the second flapping cycle.

In Figs. 19(j)-(l), the open angle of attack occurred as the wing flapped downward. This synchronized motion had a unique effect on force generation, which was recorded and shown in Fig. 20. The air vortex around the wing emerges and disappears according to the synchronization of the flap-and-twist motion every three flapping cycles, resulting in a repetition of thrust and lift in the same period. This repetition of force in three flapping cycles is unique and produces the highest thrust compared to the other models. Fig. 20 shows that lift has a positive value in a range of 0-0.06 N in both upstroke and downstroke. The thrust fluctuation is in a range of ± 0.10 N in the first cycle. In addition, the lift is also positive most of the time. The lateral force oscillation is in a range of ± 0.04 N.

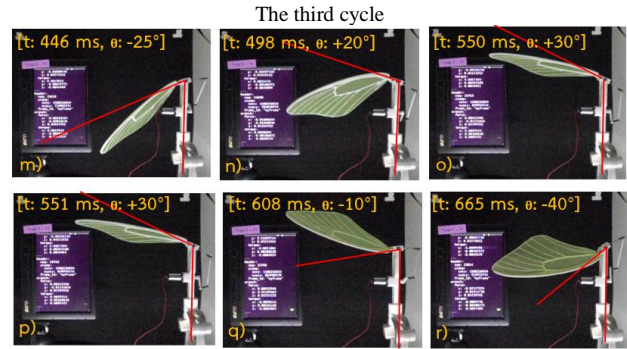


Figure 19. The repeated three-cycle flapping motion with the passive twist angle range $[-75^\circ, 75^\circ]$.

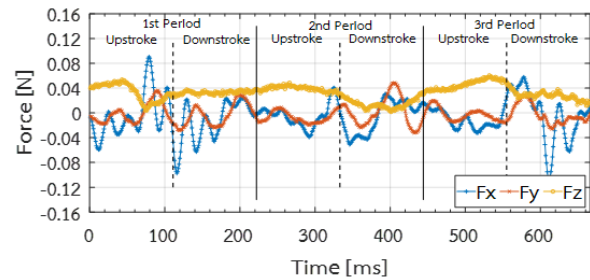


Figure 20. The flapping force components of the Model 6 with the passive twist angle $[-75^\circ, 75^\circ]$.

For ease of comparison, the flapping force components of all tested models are shown in Fig. 21. The large symmetrical passive twist wing, Model 6, generates the highest oscillatory thrust. Model 6 has the lowest oscillatory lateral force, which could be compensated by the simultaneous flapping of the left and right wings. In addition, the Model 6 generates positive lift in both upstroke and downstroke. This is the key to force generation, which allows a robot to fly by the lift force at low flapping frequency, as the butterfly does. For this reason, a large passive twist angle combined with an active flapping model like the Model 6 is the best candidate for developing a butterfly robot.

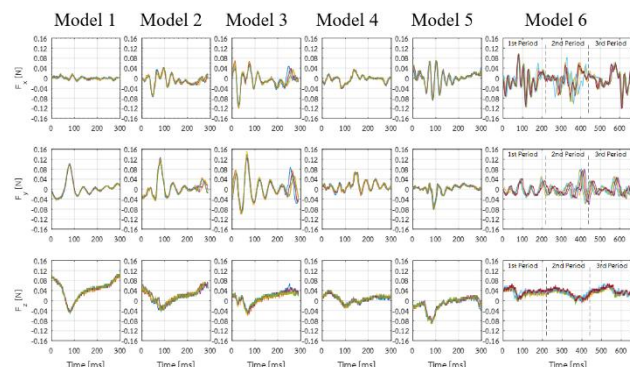
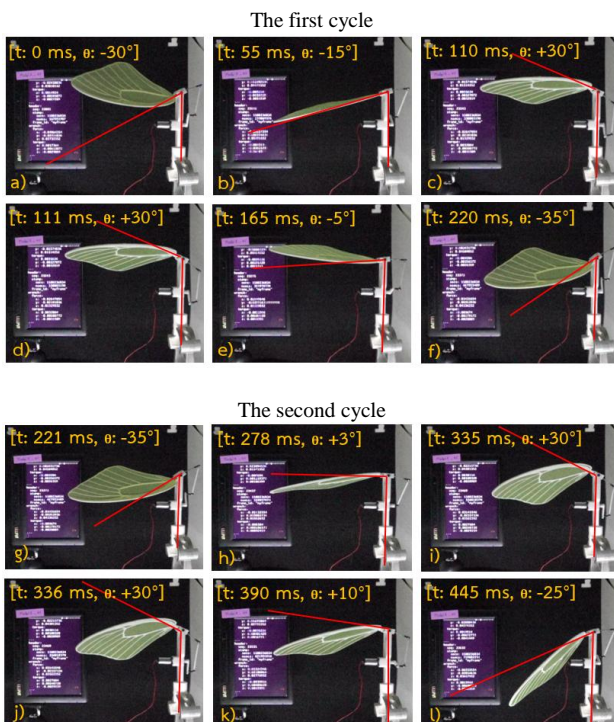


Figure 21. The comparison of the repeated flapping force components of all flap-and-twist wing models.

Based on the candidate model (Model 6), the changes in flapping and twisting angles are plotted as shown in Fig. 22. The result shows that the flapping angle varies consistently between -40° and 30° . The twist angle varies roughly in a range between -75° and 75° , which is related

to the open and closed angles of attack, respectively. In the first period, the wing begins with the closed angle of attack (twist angle of 37.5°) and gradually turns to the open angle of attack until it reaches the largest open angle of attack (twist angle of -75°) at the top upstroke. The wing can reach the largest open angle of attack at the transition from upstroke to downstroke at any flapping period, which is normally the case when the wing trailing edge follows the wing leading edge. Unique to the Model 6 is that the proposed flap-and-twist mechanism can keep the wing in the open angle of attack (negative twist angle) during the transition between the second and third periods, increasing the time to generate positive lift.

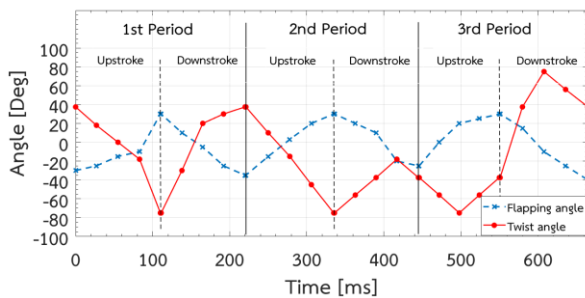


Figure 22. The relationship between the flapping angle and twisting angle of the Model 6.

VI. CONCLUSION

This is the first work to investigate the influence of the butterfly forewing flap-and-twist motion on the generation of thrust and lift. The six models of butterfly forewing with flap-and-twist mechanism were studied to investigate the wing motion and the lift and thrust generation. The flapping motion of the forewing and the generated force were recorded synchronously by using a high-speed camera and a three-axis force and torque sensor. The results of all tested models were discussed and compared. It was found that the Model 6, with a large symmetrical twist angle [-75° 75°], has a unique repetition of three flapping cycles that generates positive lift in a range of 0-0.06 N with a high thrust fluctuation of ± 0.10 N in both upstroke and downstroke. This is because the large symmetrical passive twist angle creates a unique wing motion where the angle of attack opens as the wing flapping downward, unlike the other models where the trailing edge of the wing always follows the leading edge of the wing. This discovery is the explanation for butterfly flight in nature: butterflies can rise themselves with such a low flapping frequency because positive lift is generated in both upstroke and downstroke. The proposed forewing design with active flapping and passive twisting can be used as a guiding concept for further development of a butterfly robot.

In addition, the non-twist flapping, like Model 1, produced the highest lift of 0.10 N by using the structural rigidity of the wing to resist the air drag, which can be applied in gliding flight. The high thrust can be generated by flapping with a narrow symmetrical twist angle, as in Model 2 with a twist angle of [-45° 30°], which can generate a maximum thrust of 0.04 N and a maximum lift

of 0.08 N, which is suitable for forward flight. Moreover, the adjustable range of passive twist angle could be a viable solution to mimic butterfly flight for both lift and glide.

In a future work, a hindwing will be integrated into the flapping wing system. This will also influence the aerodynamics of thrust and lift, as the overlap area of the forewing and hindwing can be varied. The study may provide an understanding of how to effectively control the wing area during flapping. After that, aerodynamic parameters such as Reynolds number, reduced frequency, and wing loading could be studied to design and optimize the weight of the body structure and motor of a flying butterfly robot.

CONFLICT OF INTEREST

All authors declare no conflicts of interest.

AUTHOR CONTRIBUTIONS

Kamonrat Tangudomkit conducted the research and drafted the manuscript; Pruittikorn Smithmaitrie is the principal investigator and corresponding author, analyzed the data, revised the manuscript. All authors had approved the final version.

FUNDING

This research was supported in part by National Science, Research and Innovation Fund (NSRF) and Prince of Songkla University (Grant No. ENG6601312S). The authors gratefully acknowledge the graduate research scholarship from Faculty of Engineering, Prince of Songkla University. The authors gratefully acknowledge the support of the Smart Mechatronic Research Unit, Faculty of Engineering, Prince of Songkla University, which made the high-performance measurement device possible.

REFERENCES

- [1] S. Deng, M. Percin, and B. van Oudheusden, "Aerodynamic characterization of 'DelFly Micro' in forward flight configuration by force measurements and flow field visualization," *Procedia Engineering*, vol. 99, pp. 925–929, 2015, doi: 10.1016/j.proeng.2014.12.623.
- [2] M. F. Bin Abas, A. S. Bin Mohd Rafie, H. Bin Yusoff, and K. A. Bin Ahmad, "Flapping wing micro-aerial-vehicle: Kinematics, membranes, and flapping mechanisms of ornithopter and insect flight," *Chinese Journal of Aeronautics*, vol. 29, no. 5, pp. 1159–1177, Oct. 2016, doi: 10.1016/j.cja.2016.08.003.
- [3] T. Kizu, M. Inoue, K. Yoshino, and K. Hiraki, "Development of Dragonfly-Like Flapping Robot," in *Proc. 2016 4th Intl Conf on Applied Computing and Information Technology/3rd Intl Conf on Computational Science/Intelligence and Applied Informatics/1st Intl Conf on Big Data, Cloud Computing, Data Science & Engineering (ACIT-CSII-BCD)*, Las Vegas, NV, USA, Dec. 2016, pp. 87–92. doi: 10.1109/ACIT-CSII-BCD.2016.028.
- [4] T. Fujikawa, K. Hirakawa, S. Okuma, T. Udagawa, S. Nakano, and K. Kikuchi, "Development of a small flapping robot," *Mechanical Systems and Signal Processing*, vol. 22, no. 6, pp. 1304–1315, Aug. 2008, doi: 10.1016/j.ymsp.2008.01.008.
- [5] B. H. Chen, L. S. Chen, Y. Lu, Z. J. Wang, and P. C. Lin, "Design of a butterfly ornithopter," *Journal of Applied Science and Engineering*, vol. 19, no. 1, Jan. 2016, doi: 10.6180/jase.2016.19.1.02.

- [6] L. Tudose and C. Budaciu, "Design and implementation of a butterfly robot system," in *Proc. 2019 24th IEEE International Conference on Emerging Technologies and Factory Automation (ETFA)*, 2019, pp. 1665–1668.
- [7] H. Huang, W. He, Z. Chen, T. Niu, and Q. Fu, "Development and experimental characterization of a robotic butterfly with a mass shifter mechanism," *Biomimetic Intelligence and Robotics*, vol. 2, no. 4, p. 100076, 2022.
- [8] P. R. Bhayu, Q. V. Nguyen, H. C. Park, N. S. Goo, and D. Byun, "Artificial Cambered-wing for a Beetle-mimicking flapper," *J Bionic Eng.*, vol. 7, no. S4, pp. S130–S136, Dec. 2010, doi: 10.1016/S1672-6529(09)60226-2.
- [9] R. J. Wood, "Liftoff of a 60mg flapping-wing MAV," in *Proc. 2007 IEEE/RSJ International Conference on Intelligent Robots and Systems*, San Diego, CA, USA, Oct. 2007, pp. 1889–1894. doi: 10.1109/IROS.2007.4399502.
- [10] N. Gans, A. Chakravarthy, and R. Albertani, "Analysis of kinematics and dynamics of Butterflies in natural flight, with estimation of occluded data," [Online]. Available: https://homepages.inf.ed.ac.uk/rbf/VAIB08PAPERS/vaib8_gans.pdf
- [11] K. Senda, T. Obara, M. Kitamura, N. Yokoyama, N. Hirai, and M. Ima, "Effects of structural flexibility of wings in flapping flight of butterfly," *Bioinspir. Biomim.*, vol. 7, no. 2, p. 025002, June 2012, doi: 10.1088/1748-3182/7/2/025002.
- [12] Y. H. J. Fei and J. T. Yang, "Importance of body rotation during the flight of a butterfly," *Phys. Rev. E*, vol. 93, no. 3, p. 033124, Mar. 2016, doi: 10.1103/PhysRevE.93.033124.
- [13] K. B. Lua, T. T. Lim, and K. S. Yeo, "Scaling of aerodynamic forces of three-dimensional flapping wings," *AIAA Journal*, vol. 52, no. 5, pp. 1095–1101, May 2014, doi: 10.2514/1.J052730.
- [14] M. Kovac, D. Vogt, D. Ithier, M. Smith, and R. Wood, "Aerodynamic evaluation of four butterfly species for the design of flapping-gliding robotic insects," in *Proc. 2012 IEEE/RSJ International Conference on Intelligent Robots and Systems*, Vilamoura-Algarve, Portugal, Oct. 2012, pp. 1102–1109. doi: 10.1109/IROS.2012.6385453.
- [15] A. K. Das and S. S. Hiremath, "Investigation on the thermohydraulic performance and entropy-generation of novel butterfly-wing vortex generator in a rectangular microchannel," *Thermal Science and Engineering Progress*, p. 101531, 2022.
- [16] T. Fujikawa and K. Kikuchi, "Development of a butterfly-style flapping robot with a different ratio of down and up stroke times," in *Proc. the 4th International Conference on Design Engineering and Science*, 2017.
- [17] Y. Ozawa, T. Fujikawa, and K. Kikuchi, "Analysis of turning motion for developing a butterfly-style flapping robot," *MM Science J*, pp. 2198–2204, 2018.
- [18] H. Tanaka, K. Hoshino, K. Matsumoto, and I. Shimoyama, "Flight dynamics of a butterfly-type ornithopter," in *Proc. 2005 IEEE/RSJ International Conference on Intelligent Robots and Systems*, Edmonton, Alta., Canada, 2005, pp. 2706–2711. doi: 10.1109/IROS.2005.1544999.
- [19] H. Tanaka, K. Matsumoto, and I. Shimoyama, "Design and performance of micromolded plastic butterfly wings on butterfly ornithopter," in *Proc. 2008 IEEE/RSJ International Conference on Intelligent Robots and Systems*, Nice, Sep. 2008, pp. 3095–3100. doi: 10.1109/IROS.2008.4651065.
- [20] S. P. Sane, "The aerodynamics of insect flight," *Journal of Experimental Biology*, vol. 206, no. 23, pp. 4191–4208, Dec. 2003, doi: 10.1242/jeb.00663.
- [21] L. Liu and M. Sun, "The added mass forces in insect flapping wings," *Journal of Theoretical Biology*, vol. 437, pp. 45–50, Jan. 2018, doi: 10.1016/j.jtbi.2017.10.014.
- [22] G. Van der Poorten and N. Van der Poorten, *The Butterfly Fauna of Sri Lanka*. Lepodon Books, 2016.
- [23] K. Tangudtableomkit and P. Smithmaitrie, "Aerodynamic experimental investigation and analysis of the flow and thrust generation of the flexible flat flapping wing robot," in *Proc. 2021 Second International Symposium on Instrumentation, Control, Artificial Intelligence, and Robotics (ICA-SYMP)*, Bangkok, Thailand, Jan. 2021, pp. 1–6. doi: 10.1109/ICA-SYMP50206.2021.9358247.

Copyright © 2023 by the authors. This is an open access article distributed under the Creative Commons Attribution License (CC BY-NC-ND 4.0), which permits use, distribution and reproduction in any medium, provided that the article is properly cited, the use is non-commercial and no modifications or adaptations are made.